STUDY OF WAVEFRONT RECONSTRUCTION TECHNIQUES APPLIED TO OPTICAL TESTING

by

Asad K. Abdallah

SUBMITTED IN PARTIAL FULFILMENT OF THE REQUIREMENTS FOR THE DEGREE OF MASTER OF SCIENCE IN THE PHYSICS DEPARTMENT OF THE SCHOOL OF ARTS AND SCIENCES,

AMERICAN UNIVERSITY OF BEIRUT
BEIRUT, LEBANON

BEIRUT
1967

STUDY OF WAVEFRONT RECONSTRUCTION TECHNIQUES APPLIED TO OPTICAL TESTING

ABDALLAH

ACKNOWLEDGEMENTS

The author wishes to express his deep gratitude to his advisor, Dr. George Ameer, for suggesting the subject and for his guidance and encouragement throughout the work.

Mr. Peter Cervenka has kindly read a part of the manuscript and made helpful suggestions.

Mr. George Majdalani and Mr. Pierre Jamous have contributed to the final form of the work: the first through the neat reproduction of the figures, and the second through the meticulous care in typing.

Finally, the generous financial support of the A.U.B. Physics Department, in providing free services, is acknowledged.

A B S T R A C T

Some classical procedures for testing optical components are reviewed; the limitations of the tests considered are indicated. A simple account of some wavefront reconstruction techniques follows. Finally an attempt has been made to indicate how these techniques can be put to use in optical testing.

TABLE OF CONTENTS

		Page
	ABSTRACT	iv
	LIST OF FIGURES	vi
I.	INTRODUCTION	1
II.	SOME WELL-KNOWN METHODS OF TESTING OPTICAL SURFACES AND COMPONENTS	3
III.	WAVEFRONT RECONSTRUCTION TECHNIQUES	39
IV.	APPLICATION OF WAVEFRONT RECONSTRUCTION TO OPTICAL TESTING	78
	REFERENCES	88

LIST OF FIGURES

Figure		Page
1.	Testing of a Spherical Mirror by the Knife-Edge Test	6
2.	Knife-Edge Method Used for Testing a Parabolic Mirror	6
3.	Geometry of the Gaviola Test	10
4.	Effectively Coincident Pinhole Source and Knife-Edge	10
5.	The Hartmann Test Illustrated by a Lens with a Raised Intermediate Zone	15
6.	Testing of a Flat Surface by Fizeau Fringes	17
7.	Haidinger Fringes Used to Test a Thick Plate	21
8.	The Twyman-Green Interferometer	24
9.	Testing of a Positive Lens with the Twyman-Green Interferometer	27
10.	An Arrangement for Testing a Concave Mirror with the Twyman-Green Interferometer	27
11.	The Principle of the Wave-Shearing Interferometer	31
12.	Origin of Scatter Fringes	35
13.	Gabor's Method of Imaging by Reconstructed Wavefronts	42
14.	The H-D Curve	45
15.	Producing the Hologram of a Semi-Transparent Object (Oblique Incidence)	51
16.	Producing the Hologram of an Opaque Object	55
17.	Wavefront Reconstruction and Image Formation from a Hologram	58

Figure		Page
18.	Linear Phase Shifts Produced by Prismatic Deflections	61
19.	Hologram of a Small Hole in an Opaque Screen	64
20.	Reconstruction of the Real and Virtual Images of a Small Hole	67
21.	Phase Shift due to a Perfect Negative Lens	69
22.	Wavefront Reconstruction with Obliquely Incident Plane Wave	73
23.	Testing a Spherical Mirror Using the Methods of Wavefront Reconstruction	81
24.	Preparation of a Hologram to be Used in the Testing of a Spherical Mirror	85

I. INTRODUCTION

In recent years there has been increased interest in producing large aperture optical systems of high resolving power. These systems are demanded by modern technology for such purposes as: aerial photographic mapping; ground, or astronomical observation from earth satelites; and optical radar using laser sources to mention just a few.

In the design of such systems the use of aspheric elements seems necessary to control aberrations. Although it is fairly easy for the optical designer to produce an aspheric element in his computer, the optical shop has more trouble producing the physical reality. Much of the difficulty, in producing aspheric elements in the optical shop, centers around testing the element to determine its figure.

The classical procedures of testing optical components usually rely on the fact that the element by itself, or in combination with a small number of other elements, can produce a good axial image of a point object. For optical designs employing a large number of elements, many of which are aspheric, this condition is no longer satisfied.

It then becomes necessary to examine such surfaces, to determine their shape, without the benefit of conjugate points. Furthermore, it is now desirable to produce simple aspheric

surfaces such as astronomical paraboloidal mirrors of large size with precision greater than was heretofore necessary, because of the fact that it is now possible to use large astronomical telescopes without the confusing effects of the earth's atmosphere.

For these reasons, it is desirable, to re-examine the classical optical test procedures to see their limitations, and to see if some of the modern techniques of wavefront reconstruction can be made to serve the useful purpose of optical testing.

What appears in Section II is, then, a review of some well-known optical test procedures. Section III deals with some salient features of wavefront reconstruction. In Section IV we have attempted to point out some of those areas where the purpose of optical testing can best be met by wavefront reconstruction techniques.

II. SOME WELL KNOWN METHODS OF TESTING OPTICAL SURFACES AND COMPONENTS

A. Description of Some Optical Test Procedures

In this section some of the well known schemes for testing optical components will be discussed so that their merits and limitations may be recognized. It is convenient to distinguish between a working test intended to help in the polishing of optical components and a performance test designed to measure the quality of finished optical systems. However some tests are suitable for both purposes.

Any test has to be related to a criterion of assessment and early methods such as the Foucault Test were related to ray optics. They were designed to test the stigmatism of a beam of light after it emerges from the component under test. Later attention turned towards the shape of the wavefront emerging from an optical component. Instruments such as the Twyman-Green interferometer test these wavefronts for sphericity or planarity. In instruments such as this it is necessary to generate a reference wave to which the wave front under test can be compared.

1. The Knife-Edge Test

The knife-edge test was first discussed by Leon Foucault in 1858. According to E.H. Linfoot[1,2,3] this test is still by far the most widely used method of testing astronomical mirrors and other high quality optical systems of large aperture during the process of optical figuring. It is of unsurpassed simplicity and sensiti-

vity when stigmatism is the property to be tested. For then the the interpretation of the test is so easy as to be almost intuitive.

Figure 1 illustrates how the test is used for testing a spherical mirror. A pinhole S, placed laterally adjacent to the center of curvature C, of a mirror M, is illuminated with light focussed by a lens. According to geometrical optics the cone of light from S to the mirror is reflected so as to pass through a point K. If the eye of the observer E is placed just behind K, and a knife-edge is moved laterally across K, then according to ray theory it is expected that the face of the mirror will grow suddenly dim as the knife edge reaches K, provided the mirror is perfect.

In the case of a parabolic mirror one of several possible arrangements used is shown schematically in Figure 2. Here F is the focus of the parabolic mirror, P is a plane parallel plate lightly silvered on the front face.

A similar arrangement to that of figure 1 may be used to test a telescope objective lens except that the lens which replaces M has to be backed by a plane mirror. Evidently the optically flat mirror has to be perfect to the accuracy expected of the component under test in both cases. If the mirror or lens is not perfect, then, as the knife-edge is moved across the position of best focus, the defect will show itself by appearing differently from the correct parts of the component.

Ray theory can not explain some of the observed effects related to the wave nature of light, but when large errors are present these

Fig. 1.--Testing of a spherical mirror by the Foucault knife-edge test (schematic).

Fig. 2.--Knife-edge method used for testing a parabolic mirror with the help of a half silvered optical flat (schematic).

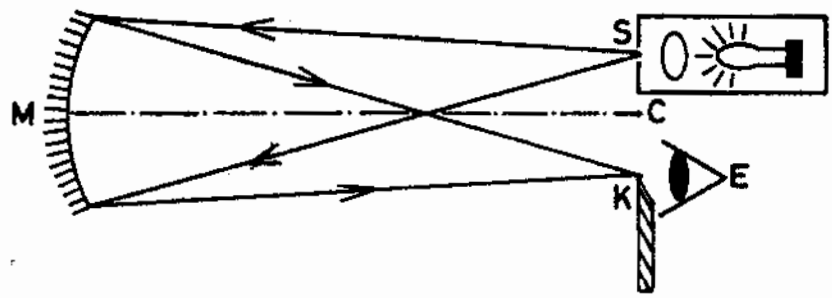

Fig. 1

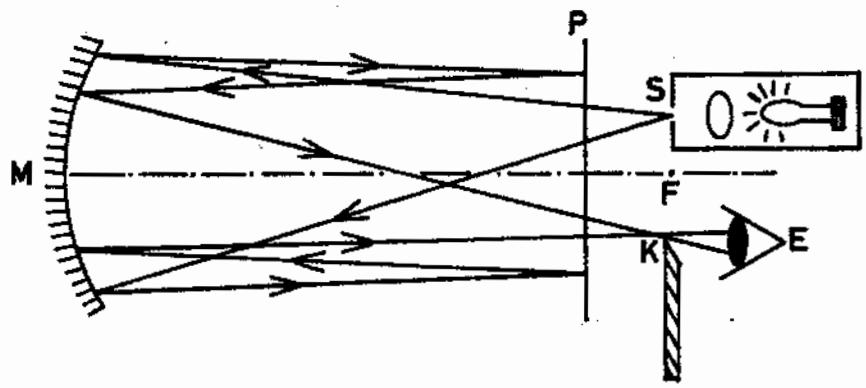

Fig. 2

effects can be disregarded without impairing the usefulness of the test. As the errors are reduced by further polishing these effects become more disturbing. To give an example, a brilliant line of light around the rim of the component often causes trouble to the inexperienced worker through being taken to indicate the presence of a steep, narrow-turned edge. Also, dark fringes appear on the brightly lit areas of the component under the test. Fortunately, their characteristic behavior as the knife edge is moved from side to side makes it easy to distinguish these diffraction fringes, which rapidly appear and disappear in different positions as the knife edge is moved, from true knife edge shadows, which change their form and intensity much more slowly.

The wave theory of the knife-edge test was studied by Rayleigh (1917), Zernike (1934) and was extended by Linfoot in two papers[1,2]. Linfoot studied the distribution of light across a plane near to the plane of best focus both for a perfect component and for a component with certain specified aberrations. He showed that (a) when a mirror is defective by more than a few wavelengths the geometric interpretation of the test gives correct information concerning the areas to be repolished; (b) the test is still useful for improving a surface which is correct to about the wavelength of light used λ, but the interpretation of the shadows is not as simple as ray theory suggests; (c) a perfect mirror will give a bright circle at the edge; (d) the test is sensitive enough to detect imperfections of surface which are of the order of $\frac{1}{40}\lambda$ deep.

Thus it appears that the knife-edge test as developed by Linfoot is highly sensitive both as a performance and as a working test. However, for testing a parabolic mirror it is necessary to have a precise optical flat of nearly the same aperture. Such an optical flat is very difficult to make when the parabolic mirror is of the size now used in leading observatories (more than 100 inches in aperture). In fact we see that the knife-edge test is most useful when the surface under test should form a point image of a point object. This drawback is remedied but not without introducing other difficulties in the modification due to E. Gaviola as described in the next section.

2. The Gaviola Test - Caustic Test

The caustic test was devised by E. Gaviola[4] and is a modification of the knife-edge test applied to the examination of a parabolic mirror (or for that matter any aspheric mirror) with errors symmetrical about the optical axis, a fairly realistic assumption. This test is based on the fact that the centers of curvature, in the plane of a diametrical section through the center of an aspheric mirror, lie on a curve called the caustic. For example, the facet of the parabola Δv_i of Fig. 3 has its center of curvature at the point (p_i, q_i) in the coordinate system shown. The relationship between these caustic coordinates (p_i, q_i) and the parabola's coordinates (x_i, y_i) are given by the calculus and coordinate geometry as

$$p_i = \frac{3y_i^2}{2r_o} \quad , \quad q_i = 2x_i \left(\frac{dx}{dy}\right)_i = \frac{y_i^3}{r_o^2} \quad , \qquad (1)$$

Fig. 3.--Geometry of the Gaviola test. PR is the true facet normal, PE is the observed facet normal.

Fig. 4.--Effectively coincident pinhole source and knife-edge for use with the Gaviola test.

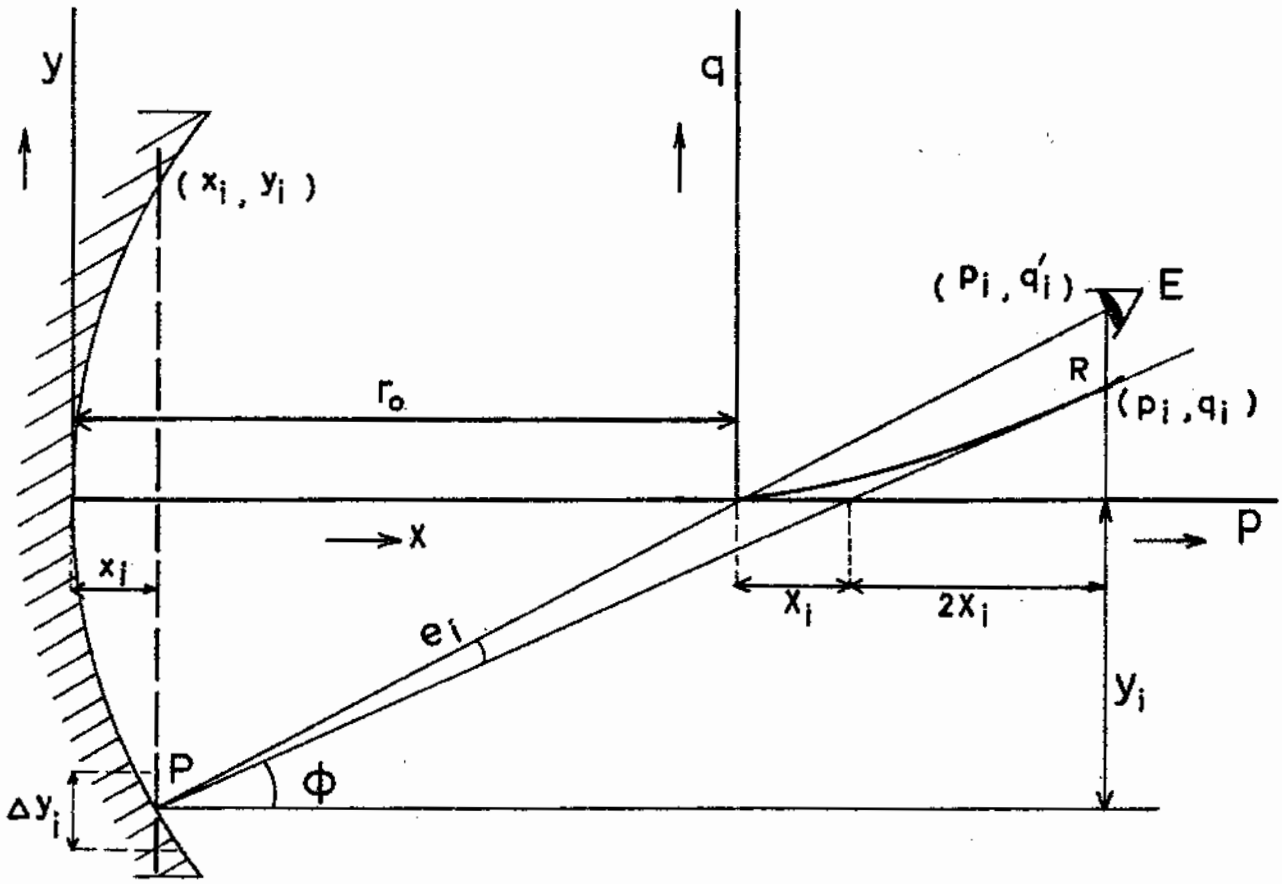

Fig. 3

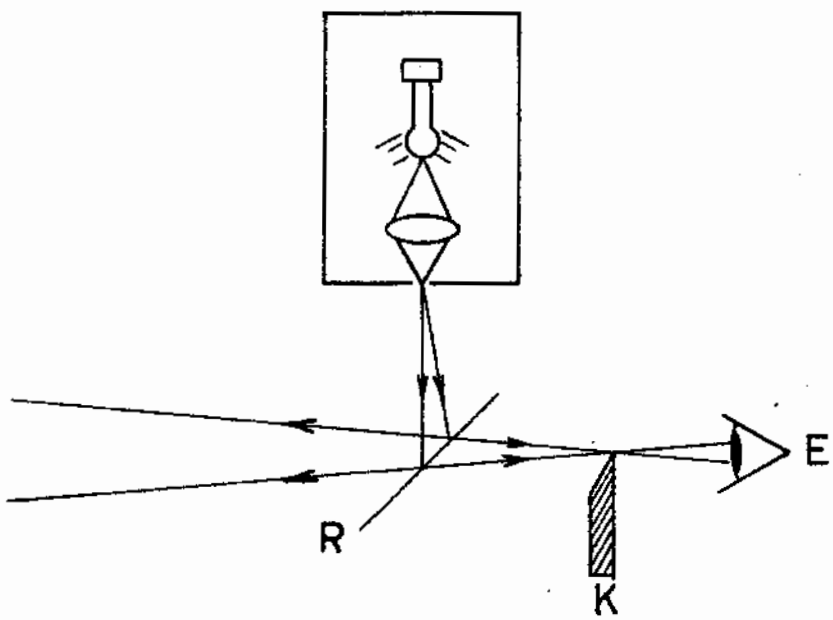

Fig. 4

where r_o is the radius of curvature at center of mirror.

A Gaviola test of a parabolic mirror involves the following steps to determine the inclination of each facet to the correct parabolic facet. For a particular one of these facets centered at y_i the coincident source and knife gadget, shown in Fig. 4, is set at the position where the center of curvature of the facet should lie if the parabolic mirror were true, i.e. at (p_i, q_i). If this zonal facet at y_i has the correct inclination then the source-and-knife should lie on its local center of curvature; whether this condition is met or not can be determined by observing the knife edge shadow on the facet. If the mirror is not a true parabola the source-and-knife must be moved, say to q_i', in a direction perpendicular to the optical axis. Here the light reflected by Δy_i will be returned on itself and $(q_i' - q_i)$ determines the angle of deviation, e_i shown in Fig. 3. After all the deviations, e_i, have been determined, we may calculate the curve of the mirror surface.

At each facet the linear increment of deviation is $e_i \Delta y_i$. The aggregate deviation at y_i is given by

$$T_{y_i} = \sum_{k=1}^{k = \frac{y_i}{\Delta y_i}} (e_k \Delta y_k) \qquad (2)$$

where T_{y_i} give the depth of the material to be removed at y_i.

The procedure of determining the e_i's consist of the following steps. To begin with, by means of the 'coincident' pinhole light source and knife-edge of Fig. 4, we determine r_o for the central zone of the

parabola. Secondly, with r_o known, Equation (1) gives the coordinates (p_i, q_i) of the point R on the caustic corresponding to y_i. Thirdly, we move the knife-edge device to the calculated point (p_i, q_i) for testing the facet at y_i. Then we make the further shift to q_i' at p_i so that the knife-edge device is brought to lie on the normal to the facet. The angle of deviation e_i is, evidently, given by

$$e_i = \frac{(q_i' - q_i) \cos \phi}{r_i} \tag{3}$$

where ϕ is as shown in the figure and r_i is the local radius of curvature of the parabola given by the formula

$$r_i = r_o \left[(1 + (\frac{y_i}{r_o})^2 \right]^{\frac{3}{2}} \tag{4}$$

This procedure is repeated for all the facets of the mirror, so that its shape may be determined by the sum given in equation (2). The zonal errors in the figure of the mirror are best seen and located if the facets, Δy_i, are small compared to the width of these error zones, In which case very narrow zonal errors can be seen with much greater sensitivity than when they are examined with the arrangement shown in Fig. 2. Furthermore, the auxiliary optical flat required in the standard knife edge test is dispensed with. However, because of the small facets required there is considerable difficulty with diffraction effects in determining the location of the center of curvature of each facet.

3. The Hartman Test

The Hartman test is a simulation of theoretical ray tracing. Its principle may be understood from Fig. 5. An opaque screen, fitted with a row of equally spaced holes, admits well defined rays. To avoid complications due to diffraction the holes should not be too small. At various positions adjacent to the position of best focus, and on both sides of it, photographic plates are exposed. By comparison of the distribution of dots on the developed plates with the computed distribution due to a perfect lens or mirror, defective zones can be detected. The sensitivity of this test is limited by diffraction. According to Candler[5] this test is not suitable for the inspection of microscope objectives which are so small that the apertures of the Hartmann screen will produce diffraction patterns that hide the aberrations.

4. Application of Fizeau Fringes

This test is very useful for the examination of the quality of optically flat surfaces. The arrangement is schematically shown in Fig. 6. S is an extended source of approximately monochromatic light; R is a semi-reflecting optical flat; and E is the eye of the observer unaided or backed by a low power microscope. The surface to be tested is laid over a transparent test flat or it is covered by such a flat. The two surfaces form a wedge of a very small angle θ, of the order of minutes of arc. The arrangement provides a means of observing straight interference fringes if the tested mirror is flat. In any case contour fringes localized near the wedge are observed, each fringe corresponding to a constant optical path. If these fringes

Fig. 5.--The Hartmann test illustrated by a lens with a raised intermediate zone. The holes marked I in the Hartmann screen S are for identification.

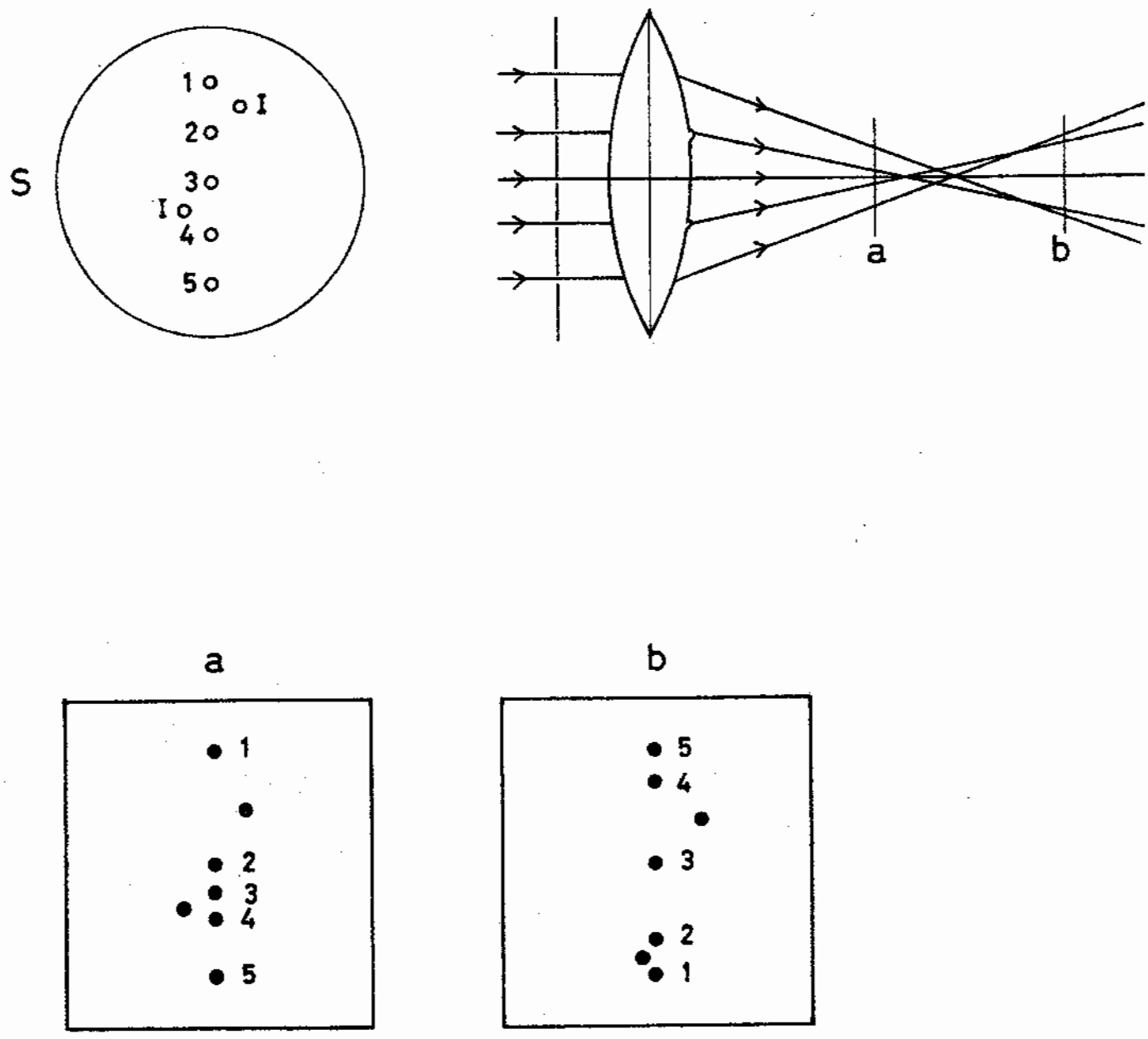

Fig. 5

Fig. 6.--Testing of a flat surface by Fizeau fringes (schematic).

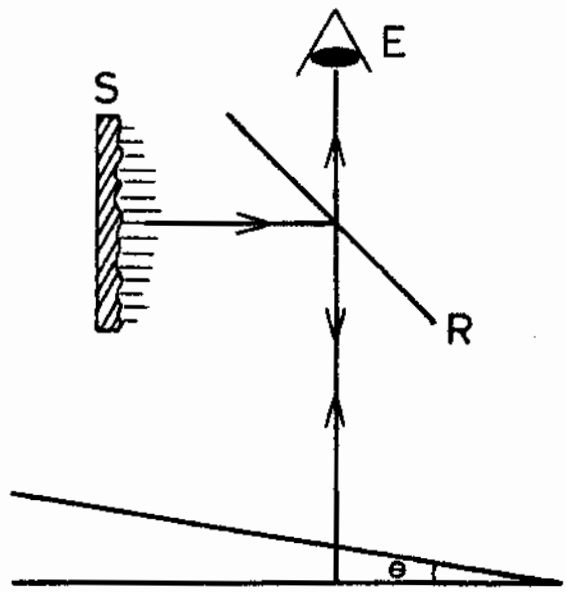

Fig. 6

are viewed from a sufficiently great distance, and if they appear parallel, straight, and equally spaced, then the tested surface is flat to the same order of accuracy as the test surface.

It can easily be shown that the separation between consecutive fringes corresponds to a change of thickness of $\lambda/2 \cos(r)$ where r is the angle of incidence and λ is the wavelength of light. Since cos (r) is very nearly constant for small r it is evident that the fringe pattern is stable under small variations from normal incidence.

According to Tolansky[6], a change of optical path of the order of $1/40\ \lambda$ can be detected by an experienced observer using this method under the most favorable conditions. It is hardly necessary to mention that the semi-reflecting flat R must be accurate.

Fizeau interference fringes are also used for proving curved lens surfaces in factory production.[7] A convex or concave lens surface is tested by placing on it a transparent matching master surface, made to specifications. Here contour fringes of the same nature as Newton rings show the error of the surface under test.

Tolansky[6,8] extended the method of contour fringes by the application of multiple beam interferometric procedures to show the details of approximately flat crystal surfaces. The same method could be applied to test a semi-reflecting plane mirror against a standard semi-reflecting optical flat of known quality. Exact parallelism must be secured between the two semi-reflecting surfaces. Optical path differences of the order of 30 angstroms are detectable due to

the tremendous increase of sharpness of fringes.

5. Application of Haidinger Fringes

Fringes produced by the interference of beams reflected at the top and bottom of a thick transparent plate are called Haidinger fringes. They are useful in testing a plane-parallel plate.[9] Since the plate is thick a highly monochromatic source of light is necessary. The arrangement used is schematically illustrated in Fig. 7. Here S is an extended diffuse monochromatic source of light, R is a beam splitter (must be optically flat), P is the plate to be tested and E is the eye of the observer, unaided or backed by a good telescopic system. If the axis of the eye or telescope is normal to the plate the observer sees circular fringes. Each circle is due to a hollow cone of light with EN (Fig. 7) as axis.

It is shown in standard books on optics that the optical path difference Δs between any two reflected rays originating from the same ray incident on the plate is given by

$$\Delta s = 2nt \cos (r) + (\lambda/2)$$

where n is the refractive index, t is the thickness of the plate, r is the angle of incidence at the lower plane surface and λ is the wavelength of light. The central ring is dark if 2nt is an integral multiple of λ and the surrounding dark rings occur at angles such that 2nt cos (r) is an integral multiple of λ. The Haidinger bands are not localized, but lie at infinity.

Fig. 7.--Haidinger fringes used to test a thick plate P (schematic).

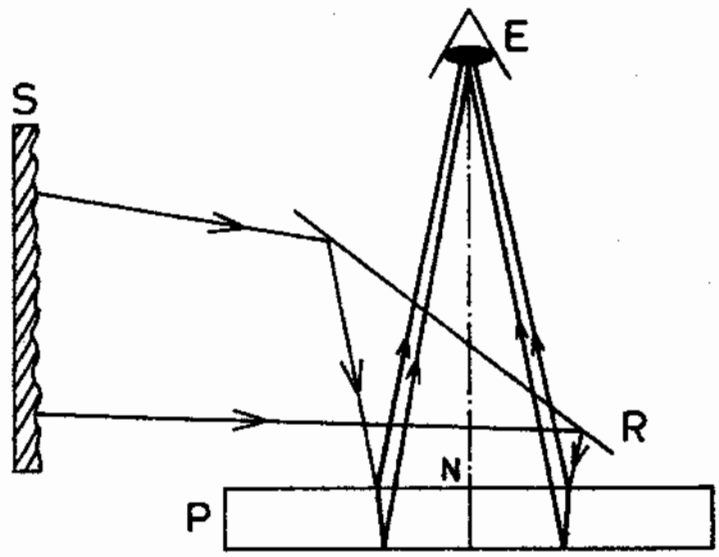

Fig. 7

If the surfaces are not parallel, there will be a change in the diameter of the circular fringes as the plate is moved parallel to its surface. These are corrected by local retouching until there is no perceptible change. Before testing for parallelism the flatness of the two surfaces must have been previously demonstrated to the desired accuracy. Distortions in the contour bands (fringes) may often be due to small differences in the refractive index.

6. The Twyman-Green Interferometer Method

When the Twyman-Green interferometer was invented in 1916, it marked a great advance in the testing of optical components. According to Candler[10] when this interferometer was used to examine the best camera lenses existing at that time, oblique rays revealed path differences of several wavelengths. Here it is pertinent to remember that the optically tolerable path difference is a quarter of a wavelength according to a Rayleigh criterion.[11] Today the best camera lenses are almost perfect as far as optical path differences are concerned. The great improvement is probably a fruit of Twyman pioneering work in optical testing.

The principle of this interferometer which is an important development of Michelson's is explained with reference to Fig. 8. A monochromatic light source is placed at the focus S of the well-corrected lens L_1, the plane wavefront emerging from L_1 is divided at the half-silvered flat R; one of the two resulting plane wavefronts is reflected back by the mirror M_1 and the other by M_2.

Fig. 8.--The Twyman-Green interferometer (schematic)

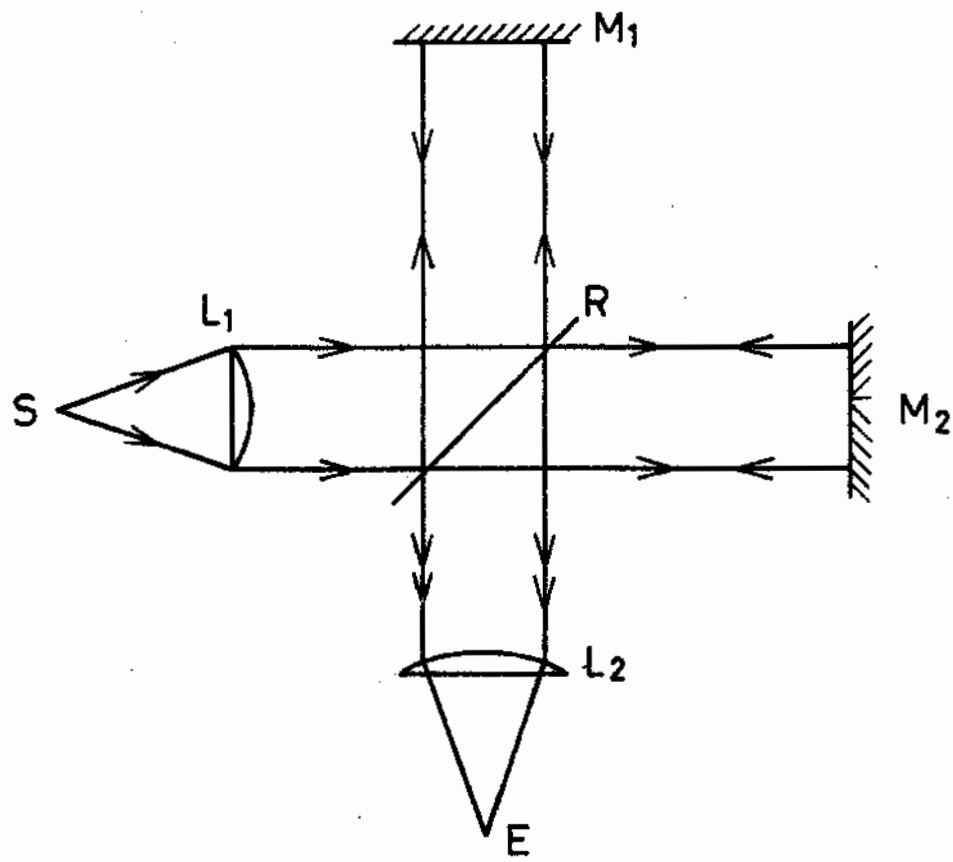

Fig. 8

The two plane wavefronts are finally incident on the lens L_2 and focused at E where the eye of the observer is placed.

Provided that the source of light is sufficiently monochromatic and optical components are perfect, the two wavefronts will interfere to produce a uniformly illuminated field if the image of M_1 in R is parallel to M_2. In other words there will be only one band in the field. If t is the distance between M_2 and the image of M_1 in R and n is the refractive index of air then the field of view will change from maximum darkness to maximum brightness as 2nt changes by half a wavelength.

As has been mentioned, the instrument is very useful in optical testing. The arrangement shown in Fig. 8 is suitable for testing an optically flat mirror which may be either M_1 or M_2, the other being of known quality. Contour fringes will be observed if the mirror under test is not perfect and they can be drawn on the surface of the mirror which is being tested. All components of the interferometer must be of high quality so that any fringe seen may be ascribed to the component under test.

For testing a lens M_2 in Fig. 8 is replaced by the arrangement shown in Fig. 9 consisting of the lens L to be examined and a good convex mirror adjusted in position such that the center of curvature of the latter is coincident with the focus of the former.

The arrangement shown in Fig. 10 may replace M_2 of Fig. 8 for testing a concave mirror with the help of a well-corrected lens L.

Fig. 9.--Testing of a positive lens with the Twyman-Green interferometer.

Fig. 10.--An arrangement for testing a concave mirror with the Twyman-Green interferometer.

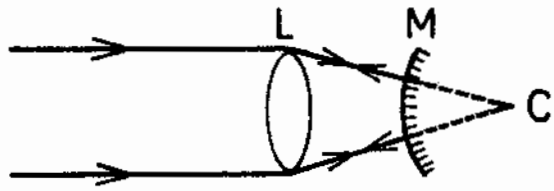

Fig. 9

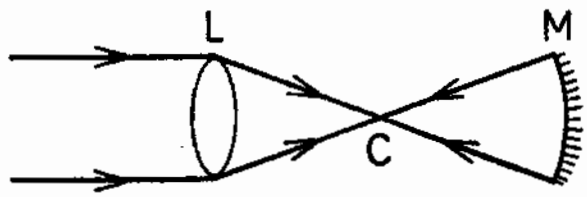

Fig. 10

To test a prism we place it between R and M_2 of Fig. 8 and tilt M_2 so that the beam incident on it is reflected back on itself. The contour fringes that appear may be eliminated by retouching the prism, but it is understood that this procedure will guarantee that the prism will behave well only if used with light having the same wavelength as that used on testing.

The adjustment of the instrument for various purposes is described in detail by Candler[12] where the limitations of the instrument are also discussed. It is important to note that the wavefront from the arm containing the component under test is compared with a plane reference wavefront from the other arm which means that whenever the former wavefront is nearly plane the Twyman-Green interferometer is very efficient. The fact that the reference wavefront has to be at least of the same aperture as the wavefront under test is a serious limitation which makes this method not suitable for testing lenses and mirrors of astronomical sizes.

An important advantage of this method is the shortness of time required to teach an optical worker how to read the contour fringes and do the retouching for nearly perfect optical components. Another advantage is that this test is highly quantitative and can be related to the Rayleigh criterion. Various interferograms (photographs of interference fringes in the field) taken in different positions of the component under test can be used to record its quality.[13]

7. Wave-shearing Interferometric Method

An important modification of the old Mach-Zehnder system was suggested by Bates in 1947 for testing nearly spherical mirrors of astronomical sizes.[14] The mirror system of this interferometer shown in Fig. 11 is the same "round the rectangle" system of Mach and Zehnder which dates back to 1891.

The idea and a practical undeveloped interferometer were presented by Bates in a meeting of the Royal Astronomical Society of England when the project of constructing a 70-inch telescope was contemplated.[15] Like many great advances, the idea is very simple and original. The principle is illustrated with reference to Fig. 11.

Consider a converging wavefront from a mirror or lens system, approaching a beam-splitter R_1. Two wave-fronts emerge from R_1, one of them is reflected by the flat mirror M_1 and the other by M_2 and finally the two wavefronts are combined by the semi-reflecting flat R_2. Initially it is arranged that the four mirrors are all parallel and positioned such that two coincident real images I_1 and I_2 are formed close to R_2. Corresponding to the incident wave-front W, two virtual emergent wave-fronts W_1 and W_2, with principal axes C_1I_1 and C_2I_2, are then exactly superimposed. An eye behind R_2 will see a field which is uniformly illuminated. R_1 and M_2 are then rotated slightly together about the principal axis of W, so that C_1I_1 and C_2I_2 are given a very small vertical displacement. Now the field becomes crossed by equidis-

Fig. 11.--The principle of the wave-shearing interferometer

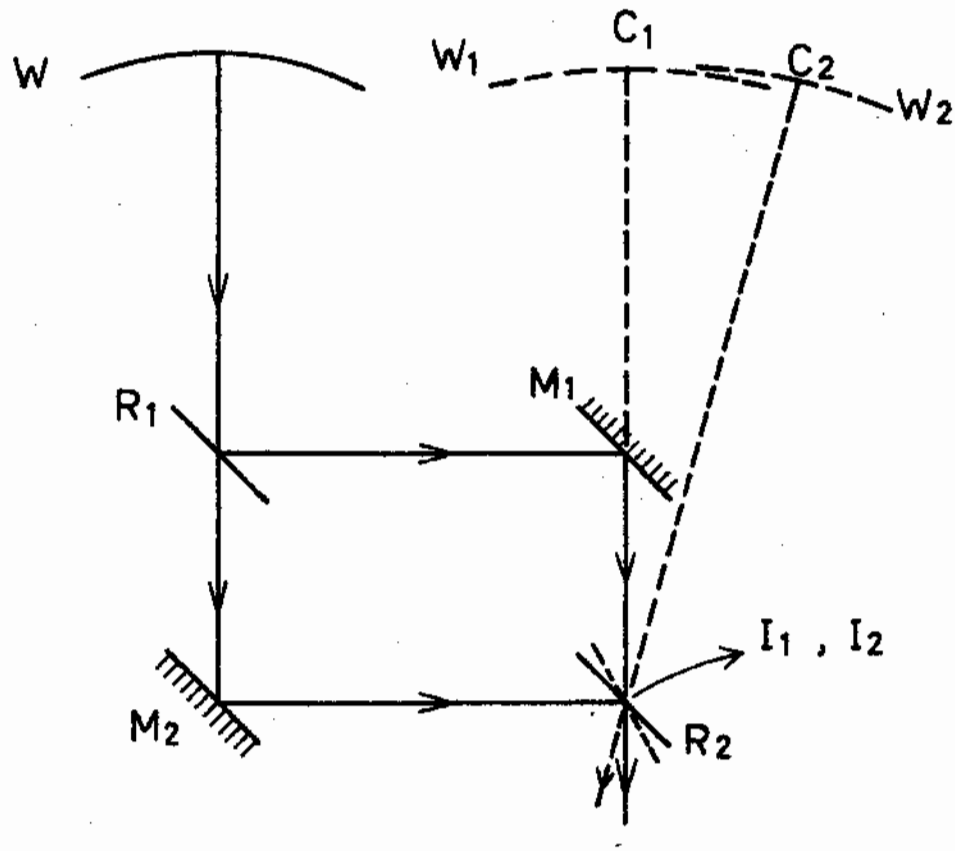

Fig. 11

tant horizontal fringes.

Next let us suppose that R_2 is rotated about a vertical axis through I_1 and I_2 (these are very close). C_1I_1 will not be affected, but C_2I_2 will be rotated by twice the angle through which R_2 is rotated and the virtual wavefront W_2 will be sheared relative to W_1.

When W_1 and W_2 are perfectly spherical the above rotation will not affect the system of fringes. In general the fringes are displaced by an amount depending on the asphericity of W. By measurement of the change in the order of the interference at a given point in the field due to a certain shear, the error in the incident wavefront from sphericity can be determined.[15]

The use of this interferometer is limited to wave-fronts which are surfaces of revolution and are either spherical or deviate from the spherical shape only slightly, for otherwise the interpretation of the change in the fringe system due to shearing becomes formidable. The main advantage gained is that no reference wavefront from a large flat is necessary to test an astronomical mirror where a star may act as the source of light and the nearly spherical wavefront reflected from the paraboloidal mirror acts as W of Fig. 11. Another advantage is the simplicity of the instrument: the testing apparatus proposed for the examination of a 70-inch telescope occupied a 6-inch cube.[15]

8. Scatter Fringes Method

To illustrate how scatter fringes can arise, consider a plane parallel back-silvered mirror with a thin layer of dust on the front and let a beam of light strike the mirror at normal incidence. Light is scattered by the dust particles and can reach the eye by two different paths as shown in Fig. 12, one being by reflection after scattering and the other by reflection before scattering. The two resulting rays are coherent since they come from the same source.

It is easy to show that the optical path difference Δs between two rays scattered at angle r is given by

$$\Delta s = 2nt\,(1 - \cos r')$$

where n is the refractive index, t is the thickness of the mirror and r' is the angle of incidence at the silvered surface. This evidently depends on the angle of scattering and vanishes as the angle of scattering goes to zero. Since the emergent rays are parallel, the fringes are located at infinity.

This phenomenon has been applied by Burch[17] to make a simple interferometer suitable for testing large spherical surfaces. Interference occurs where scattered light reflected by all parts of the mirror under test is superimposed on light reflected from a chosen small part, the latter forming the reference beam. Both beams are arranged to transverse the same optics through the use of two replicas of a specially

Fig. 12.--Origin of scatter fringes

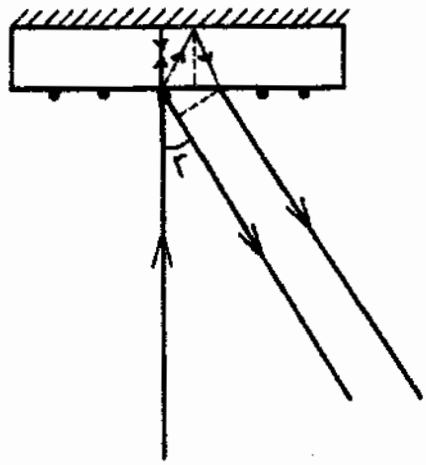

Fig.12

prepared diffusing plate. Interference is possible even with white light and the instrument is described as common path interferometer.

This interferometer described in detail by J. Dayson[18] has three advantages over the Twyman-Green interferometer. First it is very stable; secondly the source of light need not be highly monochromatic; and lastly no large high quality optical components are required to test large spherical mirrors. As indicated before the use of this method is limited to the testing of spherical mirrors or quasi-spherical wavefronts.

9. Other Interferometric Tests

Other interferometric tests for the investigation of spherical and flat surfaces are described by Dayson[19] and by Saunders[20]. The latter describes the application of Koster double-image prism, in an arrangement called a wavefront inverting interferometer, for testing a lens. Presence of various aberrations can be easily detected by inspection of the interferograms.

B. Classification of Optical Tests

It can be seen from the previous description of optical tests that they may be classified in the following manner.

1. Tests Suitable for Systems which are Capable of Forming Point Images

Systems which form a real point image of a point sourse, placed at a suitable distance, can be readily tested with the standard knife-edge test, the wavefront shearing interferometer, or the scatter fringe interferometer. These tests rely on the fact that the wavefront emerging from the optical component under test is quasi-spherical.

In the knife-edge test, the point of interest is the center of the spherical wavefront. The wavefront shearing interferometric test utilizes the symmetry of wavefronts which are nearly spherical surfaces of revolution. In the scatter fringes method the defects, if any, in an optical component of the point image type, may be detected by observing interference between a wavefront coming from a selected small part of the element under test and a wavefront coming from the whole element.

2. Tests which Require a Precise Reference Wavefront

Test procedures which require a precise reference wavefront are represented, in our account, by the Twyman-Green interferometer and the Fizeau tests. The fact that the

reference wavefront has to be of, at least, the same aperture as the wavefront coming from the examined component, restricts the usefulness of such tests to optical elements of fairly small aperture.

3. Testing of a Plane-Parallel Plate

A transparent plane-parallel plate may be readily tested by the Haidinger fringes method.

4. Tests Useful in More General Situations

The Gaviola and the Hartmann tests are, in a certain sense, applicable in more general situations. Both tests are, however, not convenient for the examination of small aperture components because of difficulties caused by diffraction effects.

The Gaviola test is useful for the examination of concave mirrors of arbitrary shape, since it essentially depends on determining the caustic curve for various sections of the mirror surface.

The Hartmann test basically depends on the comparison of the actual distribution of rays from the system under test with the computed distribution for a perfect system. This fact extends the applicability of this test, especially, in the age of high speed digital computers.

III. WAVEFRONT RECONSTRUCTION TECHNIQUES

A. The Gabor's Pioneering Work

In trying to improve the resolution of electron microscopes, Gabor[21,22,23] invented a two-step method of optical imagery. In the first step an object is illuminated with a spatially coherent monochromatic light wave. The object is chosen such that a large fraction of the wave penetrates undisturbed through it. A Fresnel diffraction pattern called a hologram, formed by the interference of the secondary waves scattered by the object with the strong coherent background wave, is recorded on a photographic plate. In the second step the plate suitably processed, is placed in the original position and is illuminated with the background wave alone. The wave which is diffracted by the plate is found to contain a component called a reconstructed wavefront which gives rise to a virtual image of the original object at the position which the object formerly occupied. However, a twin wavefront having the same amplitude but opposite phase shifts relative to the background wave is also generated. This will in general have a disturbing effect on the virtual image when the latter is viewed.

It is possible to make a real image from the reconstructed wavefront by means of optical methods. It is only necessary to send the reconstructed wave through a suitable image-forming system, in order to reconstruct the image of the object. To explain the method further we go over the two steps in more detail.

1. Producing the Positive Hologram.

Consider a monochromatic wave from a small source S, impringing on a semi-transparent object O, Fig. 13 (a). Let H be a screen a certain distance behind the object and let $U = A \exp(if)$ represent the complex disturbance at a typical point of H, A, being the real amplitude and f, the phase of the disturbance. U may be considered as the sum of two terms.

$$U = U_1 + U_2 = \left[A_1 \exp(if_1) + A_2 \exp(if_2) \right] \tag{1}$$

where $U_1 = A_1 \exp(if_1)$ represents the incident wave which is the field which would be produced at H in the absence of the object. The other term, $U_2 = A_2 \exp(if_2)$ represents the secondary, or diffracted, wave which contains information about the object.

Equation (1) may be written as

$$U = \exp(if_1)\left[A_1 + A_2 \exp i(f_2 - f_1) \right] \tag{2}$$

According to (2) the amplitude of the resultant disturbance may be written

$$A = (UU^*)^{\frac{1}{2}} = \left[A_1^2 + A_2^2 + 2A_1 A_2 \cos(f_2 - f_1) \right]^{\frac{1}{2}} \tag{3}$$

We have omitted the factor exp -iwt and thus we have implicitly assumed that the secondary wave has the same frequency as the incident wave which is usually the case.

Fig. 13.--Gabor's method of imaging by reconstructed wavefronts. (a) represents formation of the hologram; (b) represents the reconstruction.

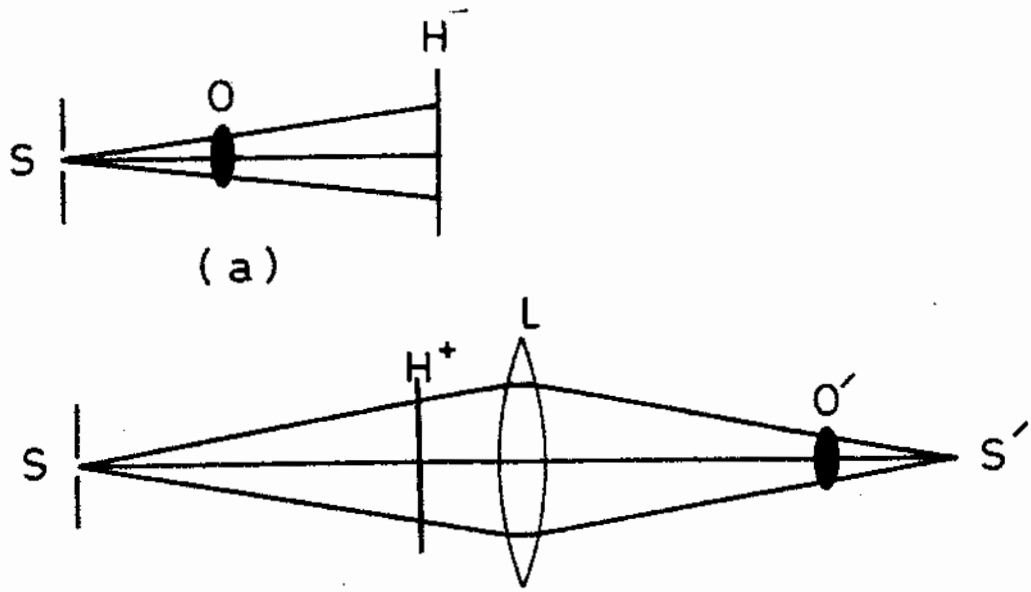

Fig.13

Next let a photographic plate be exposed in plane H. After processing let the transmittance of the plate be α. This is defined as the ratio of the complex amplitude of the wave emerging from the plate to that of the wave incident on the plate. The corresponding transmission factor for the intensity is $T = \alpha\alpha^*$; and the quantity

$$D = -\log_{10} T = -\log_{10} \alpha\alpha^* \tag{4}$$

is called the density of the plate. The product E of the intensity $I = A^2$ of light that reaches the plate and the time t of exposure

$$E = It \tag{5}$$

is called the light sum, or simply exposure, and the curve giving D vs $\log_{10} E$ is known as the Hurter-Driffield curve. This is usually S shaped as shown in Fig. 14 with a straight part in the middle, between P and Q. In the linear portion of the curve, the density D of the negative is given by

$$D = D_o + \Gamma \log_{10} \frac{E}{E_o} \tag{6}$$

where Γ is the slope and D_o and E_o are constants. Using (4), it follows that

$$T = T_o \left(\frac{E}{E_o}\right)^{-\Gamma} \tag{7}$$

where T_o is a constant.

We now make the simplification of pure absorption (without change of phase). Consequently α is real, and the transmittance α_n of the negative hologram is given by

$$\alpha_n = (K_n A)^{-\Gamma_n} \tag{8}$$

Fig. 14.--The H-D curve

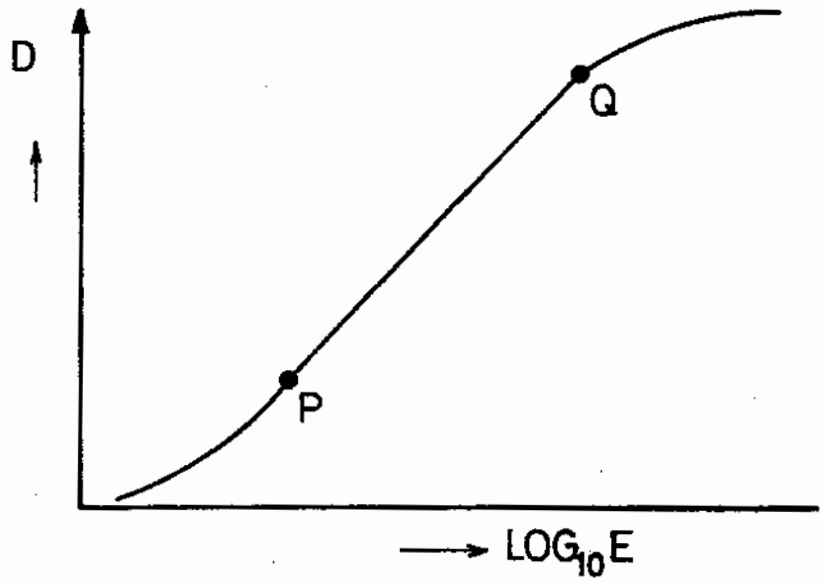

Fig. 14

where K_n is proportional to the square root of the time of exposure.

If a positive print of the negative hologram is taken, the amplitude transmission factor α_p of the positive hologram, is given by

$$\alpha_p = \left[K_p \, (K_n \, A)^{-\Gamma_n} \right]^{-\Gamma_p} = K A^{\Gamma} \qquad (9)$$

where $\Gamma = \Gamma_n \, \Gamma_p$ is the "over all gamma" of the negative-positive process and $K = K_p^{-\Gamma_p} \, K_n^{\Gamma}$.

2. The Reconstruction

In the reconstruction process (Fig. 13 (b)) the positive hologram (H^+) whose amplitude transmission factor is given by (9) is illuminated by the coherent background U_1 alone. The background is obtained simply by removing the object, otherwise keeping the geometry of the original arrangement. A substitute wave U_3 emerges from the plate, where

$$U_3 = \alpha_p \, U_1 = K A_1 \exp (i f_1) \left[A_1^2 + A_2^2 + 2 A_1 A_2 \cos (f_2 - f_1) \right]^{\frac{1}{2}\Gamma} \qquad (10)$$

As a simple case, we choose $\Gamma = 2$, and obtain

$$U_3 = K A_1^2 \exp (i f_1) \left[A_1 + \frac{A_2^2}{A_1} + A_2 \exp i(f_2 - f_1) + A_2 \exp - i(f_2 - f_1) \right] \qquad (11)$$

On comparing (11) and (2) it is seen that if A_1 is constant, i.e. if the background is uniform, the substitute wave U_3 contains a component (the first and third terms in equation (11), called the reconstructed wave, proportional to U. The remainder of (11) consists of two terms. One, the second term in (11), has the same phase as the background and an amplitude $(A_2/A_1)^2$ times that of the background. This term can be made negligibly small by making the background sufficiently strong. The other term (last term of 11) has the same amplitude as the reconstructed secondary wave but has a phase shift of opposite sign relative to the background. It is said that it represents a conjugate wave and it can be shown that it may be considered as being due to a fictitious object similar to the true object, but situated in a different plane.

Thus, provided the background is uniform and strong compared to the scattered wave, the substitute wave U_3 of equation (11) is effectively the same as the original wave, apart from a contribution arising from the conjugate object. It follows that if a lens L is placed behind the positive hologram and the hologram is illuminated by the coherent background alone (Fig. 13 (b)) an image O' of the original object will be formed in a plane conjugate to that of O, but this image will usually be degraded by a contribution due to the conjugate object. Conditions may be found under which this effect is not serious.

Such conditions were investigated by Gabor[22,23], Rogers and Bragg[24], and Kirkpatrick and El-Sum.[25] Furthermore, if two holograms are produced which are complementary in the sense that the deficiencies of one are compensated by the other, and the reconstruction is made by using both holograms together, the undesirable effect of the twin image can be completely eliminated. Such techniques are theoretically sound but experimentally they present the difficult problem of precise alignment of two holograms.[26]

B. Recent Advances in Wavefront Reconstruction

As indicated in the previous section the original idea of two-step imaging (wavefront reconstruction) is due to Gabor. The fact that the reconstructions obtained by Gabor were limited to those of small semi-transparent objects, and were not of high quality, does not mean that something was wrong with the original idea. Rather, the limination was due to the fact that it had not been otherwise possible to meet the requirement of strong coherent background with the optical sources available at that time.

With the development of the laser in 1960, a new tool became available for reconstruction techniques. This instrument is capable of generating strong monochromatic light, coherent over large areas. Thus it became possible to play with the experimental arrangements and develop the ideas of Gabor further so as to achieve better

results. This was taken up by many scientists with Leith and Upatnieks[27,28,29], and Stroke and Coworkers, [30,31,32] outstanding among them.

Greater coherence has made it possible to alter the manner of superposing the coherent background on the beam scattered by the object. The background beam is now incident obliquely on the plane of the hologram, a prism or mirror having been interposed in the path. As shown in the following two sections, which describe the production of the hologram and the reconstruction respectively, this technique does the trick of forming the conjugate images in different directions. Thus the two conjugate images are naturally separated and either of them may be viewed without the disturbing effect of the other.

1. Making The Hologram.

Fig. 15 illustrates the method of making the hologram of a semi-transparent object. A plane wave from a laser illuminates the object O and after scattering the transmitted complex wavefront w_2 travels towards the photographic plate H. Above the object a transparent wedge P deviates the upper part of the plane wave by an angle θ and the reference plane wavefront w_1 travels towards H where the fields due to w_1 and w_2 are superposed.

Fig. 15.--Producing the hologram of a semi-transparent object (oblique incidence).

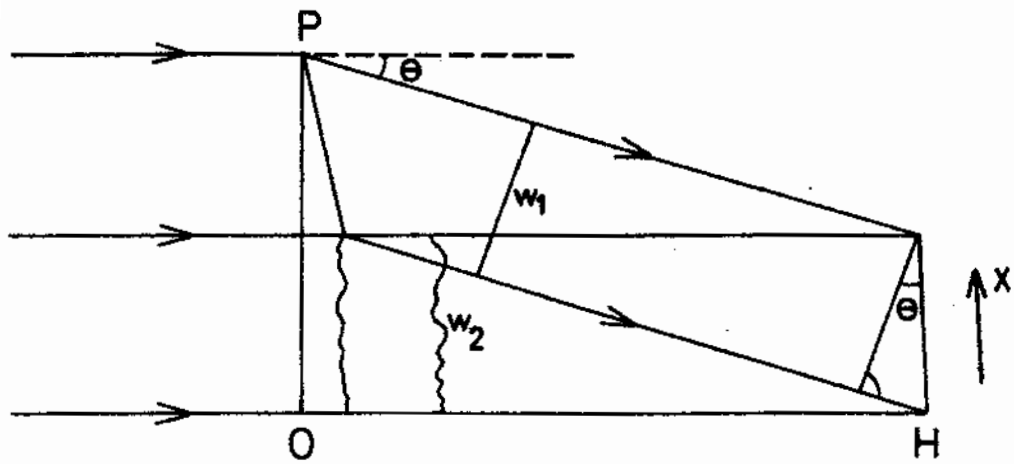

Fig. 15

At the photographic plate the field due to the reference plane wave may be represented by $A_o \exp(-iax)$ where A_o is the amplitude, x is as shown in the figure and

$$a = \frac{2\pi}{\lambda} \sin\theta \doteq \frac{2\pi}{\lambda}\theta \qquad (12)$$

where λ is the wavelength of light and the approximation holds for small θ. For simplicity we assume that the field at a point on H due to the scattering object to depend only on x and hence we may represent it by $A(x) \exp if(x)$, where $A(x)$ is the amplitude and $f(x)$ is the phase. (A factor exp -iwt is omitted throughout.)

Thus the resultant field E at the photographic plate may be represented by

$$E = A_o \exp(-iax) + A(x) \exp(if(x)) \qquad (13)$$

The emulsion of the photographic plate is sensitive to the intensity $I = EE^*$, where E^* is the complex conjugate of E. Using (13) we find

$$I = A_o^2 + A(x)^2 + 2A_o A(x) \cos(ax + f(x)) \qquad (14)$$

In the linear portion of the H - D curve the amplitude transmittance $\alpha(x)$ of the developed photographic plate will be given by

$$\alpha(x) \propto (I(x))^{-\frac{\Gamma}{2}} \qquad (15)$$

where Γ is again the slope. Substituting for $I(x)$ from Equation (14) we see that $\alpha(x)$ may be represented by

$$\alpha(x) = \left[A_o^2 + A(x)^2 + 2A_o A(x) \cos\,(ax + f(x))\right]^{-\frac{\Gamma}{2}} \qquad (16)$$

Assuming that $A(x)$ is much smaller than A_o we may expand using the binomial theorem and retain the leading terms only. The result is

$$\alpha(x) \propto 2A_o^2 - \Gamma A(x)^2 - 2\Gamma A_o A(x) \cos\,(ax + f(x))$$

$$= 2A_o^2 - \Gamma A(x)^2 - \Gamma A_o A(x) \exp i(ax + f(x))$$

$$- \Gamma A_o A(x) \exp - i\,(ax + f(x)) \qquad (17)$$

The photograph whose transmittance is given by (17) is the hologram. An important remark may be made concerning the last equation. Neither the sign nor the exact value of Γ is important in the recording process. Making a contact print of the hologram, which changes the sign of Γ, will only shift the phase of the non-constant terms of the transmittance by 180^o which is of no consequence. Changing the magnitude of Γ will have the effect of multiplying each of the non-constant terms by the same factor which is again of little importance.

So far we have described how a hologram of a semi-transparent object can be made. In Fig. 16 an arrangement suitable for making the hologram of an opaque object is illustrated. Part of the incident plane wave from a laser is deviated by a plane mirror M to form the reference wavefront w_1; the other part of the incident wave is scattered by the object O and results in a complicated wavefront w_2

Fig. 16.--Producing the hologram of an opaque scattering object.

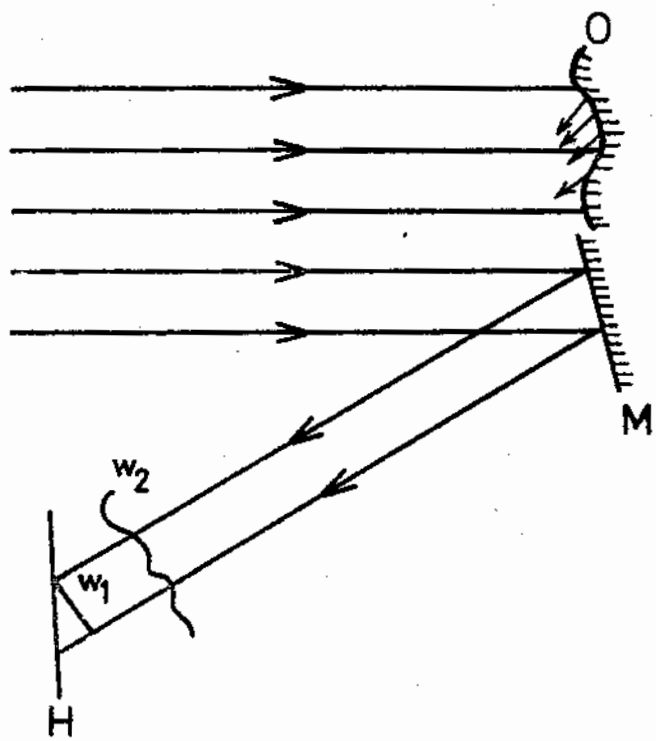

Fig. 16

striking H where the hologram is recorded. The transmittance of the hologram will be given by an equation similar to (17).

In the two examples chosen the reference beam has been a plane wave falling obliquely on the plane of the hologram. Instead of a plane wave the reference wavefront could be a spherical wave.

2. The Reconstruction Procedure

In this step the hologram is illuminated with a coherent plane wave as illustrated in Fig. 17. As the plane wave incident normally passes through the photographic plate, it is multiplied by $a(x)$ as given by Equation (17). Four distinct wavefronts corresponding to four terms of the equation above will emerge from the hologram.

The first term, being a constant, attenuates the parallel beam uniformly, but otherwise does not change it. The second term also attenuates the beam but not uniformly so that the plane wave suffers some diffraction as it passes through the hologram. The wavefronts that result from the first and second terms of equation (17) are indicated by 1 and 2, respectively, in Fig. 17.

The wavefronts produced by the third and fourth terms are more interesting. To understand how they affect the incident plane wave, reference is made to Fig. 18 where it can be seen that a triangular prism shifts the phase of a normally incident ray by an amount proportional to the prism thickness at the point of incidence. A positive phase shift deflects the ray upward, and a negative one deflects the ray downward. Thus the wavefront produced by the

Fig. 17.--Wavefront reconstruction and image formation from a hologram.

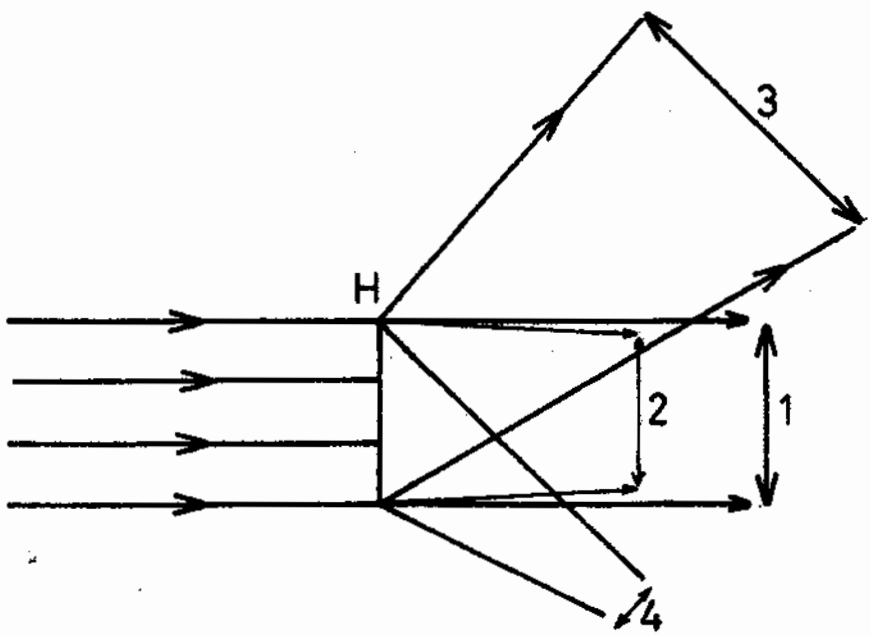

Fig. 17

third term may be interpreted as the product of the wavefront produced by the object of Fig. 15 and a positive prismatic phase shift. The fourth term may be considered to give rise to a wavefront represented by the complex conjugate of the amplitude of the original wavefront scattered by the object and a negative prismatic phase shift. The wavefronts that result from the third and fourth terms are represented by 3 and 4, respectively, in Fig. 17.

It follows that the third and fourth components of the transmittance equation (17) deflect the beam upward and downward respectively through an angle θ defined by equation 12. Moreover, in the case of the third term the upward deflected beam is also multiplied by the scattered amplitude $A(x) \exp if(x)$ and therefore a copy of this wavefront is reconstructed. This gives rise to a virtual image of the original object. However, in addition to deflecting the incident beam downwards, the fourth term multiplies it by the complex conjugate of the scattered amplitude and the result will be a real image of the scattering object. At a distance sufficiently far from the hologram the two images are naturally separated since they are formed in well-separated directions.

Fig. 18.--Linear phase shifts produced by prismatic deflections. O is the origin of x. (a) represents exp (iax); (b) represents (-iax).

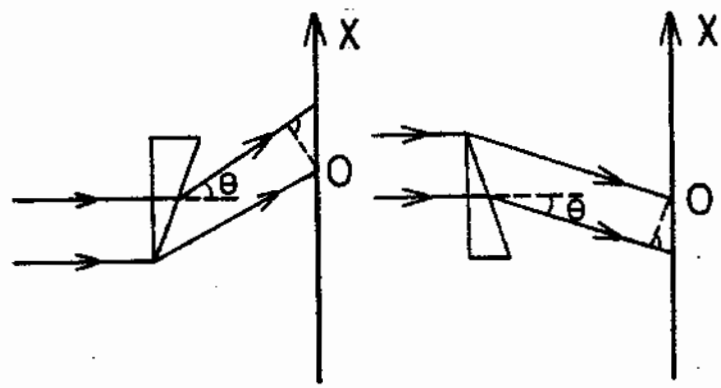

Fig. 18

3. Discussion of the Physical Principles of the Off-axis Wavefront Reconstruction Technique.

The physical principles of the technique may be illustrated by considering a small hole in an opaque plate as object, Fig. 19. When this aperture is illuminated with a plane wave it will act as a source of spherical waves according to Huygen's principle. With the reference beam shown in the figure the complex amplitude E on the photographic plate H will be of the form

$$E = A_o \exp i(-ax) + A \exp i\left(\frac{\pi}{\lambda f}\right)x^2 \qquad (18)$$

where A is the amplitude of the spherical wave generated by the small hole at the center (x=0) of the hologram, and f is shown in Fig. 19, the remaining symbols are familiar. The first term of (18) represents the plane reference wave and the second term represents the spherical wave due to the point object. The dimension of the hologram is assumed small enough for the sagitta formula to be a good approximation. (In the formula $\frac{e^{ikr}}{r}$ for a spherical wave refered to its center, r is considered constant in the denominator, over the aperture of the hologram, but not in the exponent due to the presence of the large multiplier $k = \frac{2\pi}{\lambda}$.)

By comparison of equations (18) and (13) we see that the transmittance $\alpha(x)$ of the developed hologram may be obtained from equation (17) by the transformation $A(x) \rightarrow A$, $f(x) \rightarrow (\frac{\pi}{\lambda f})x^2$. Thus the amplitude transmittance $\alpha(x)$ is now given by:

Fig. 19.--Hologram of a small hole in an opaque screen.

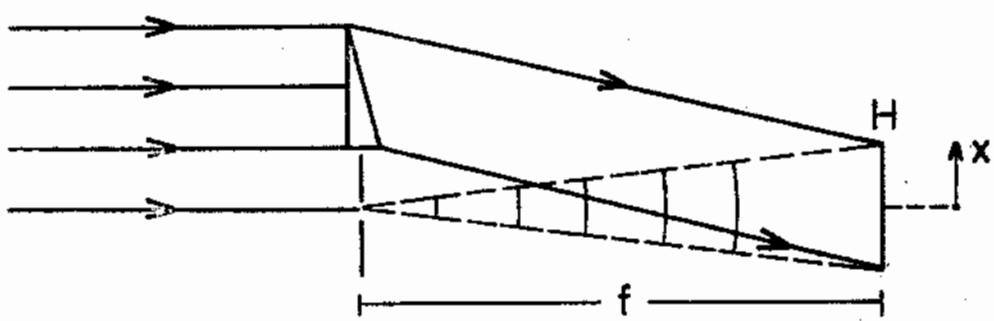

Fig. 19

$$a(x) = 2A_o^2 - \Gamma A^2 - \Gamma A_o A \exp i(ax + \frac{\pi}{\lambda f} x^2)$$

$$- \Gamma A_o A \exp - i(ax + \frac{\pi}{\lambda f} x^2) \qquad (19)$$

This formula allows us to understand the mechanism of the reconstruction process in a simple case. When the hologram described by $a(x)$ above is illuminated with a parallel beam of coherent light, three distinct components (wavefronts) are generated as in Fig. 20.

The first component is produced due to the first two terms which being constant will give rise to a transmitted plane wave with its amplitude uniformly attenuated. The third and fourth terms produce two additional components by deflecting the incident wave upward and downward, respectively, due to the linear phase shifts in their exponents.

To show that these components give rise to a virtual and a real image of the aperture we recall the action of thin, positive and negative,lenses on plane waves. Upon emerging from a perfect negative lens a plane wavefront is transformed into a divergent spherical wavefront, Fig. 21. In this Figure F represents the focus of the negative lens, O the center of the lens, and P a point on the lens a distance x from O. The two points P and O have the same phase if we consider them on the plane wavefront. The lens will advance the phase of P relative to O by $(r - f) \frac{2\pi}{\lambda}$.

Fig. 20.--Reconstruction of the real and virtual images of a small hole. In the figure W is the reconstructed wavefront, R is the real image, V is the virtual image.

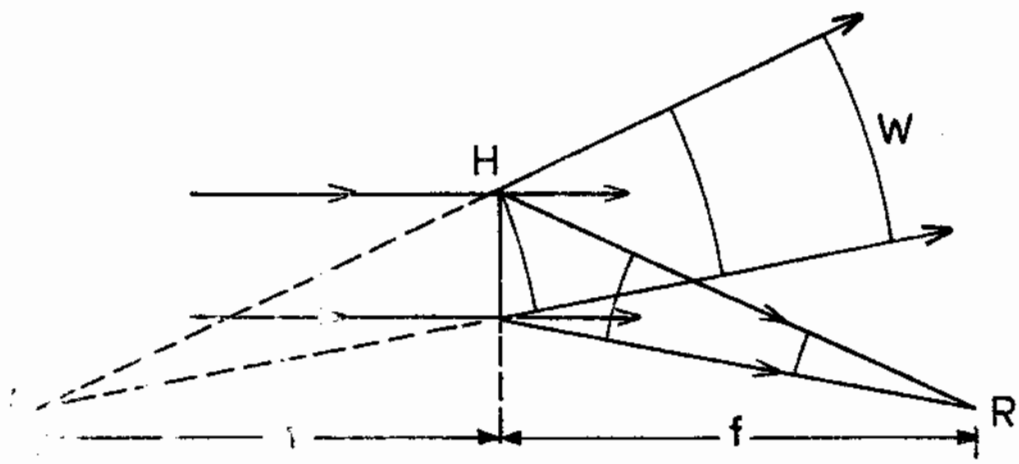

Fig. 20

Fig 21.--Phase shift due to a perfect negative lens

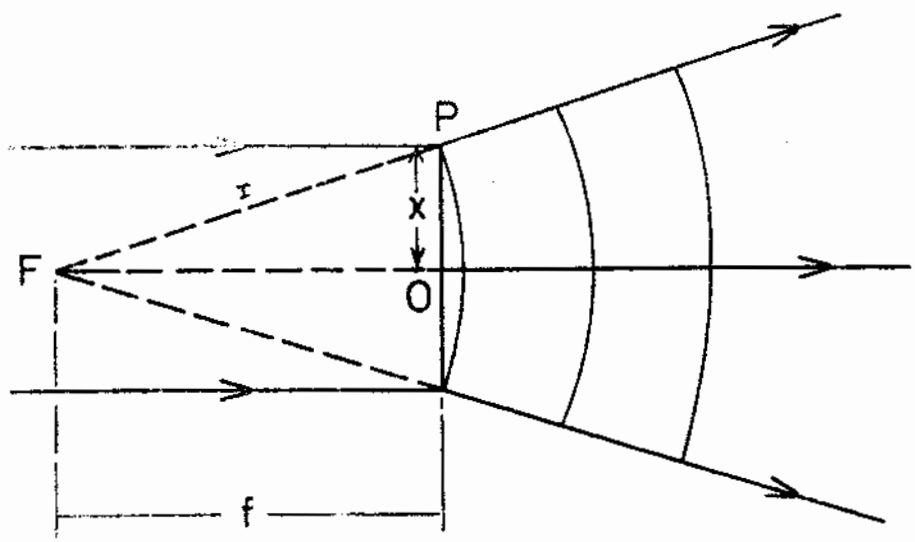

Fig. 21

Now

$$r-f = \frac{(r-f)(r+f)}{r+f} = \frac{r^2 - f^2}{2f} = \frac{x^2}{2f}$$

where f is the focal length of the lens and r is as shown in the figure. Thus the phase shift produced by a negative lens at a point distant x from its center is given by

$$\frac{\pi x^2}{\lambda f} \qquad (20)$$

Similarly for a positive perfect lens the phase shift is

$$-\frac{\pi x^2}{\lambda f} \qquad (21)$$

Returning now to the component produced by the third term of equation 19 we see that the effect of this term is to give rise to a virtual image (spherical wavefront that seems to start on the left of the hologram at a distance f). This is due to the factor $\exp(i \frac{\pi x^2}{\lambda f})$. However the rays will be displaced upward by an angle θ given by

$$a\lambda = 2\pi\theta \qquad (22)$$

Similarly the last term will give rise to a real image, in a direction making an angle θ with the axis, and at a distance f from the hologram. With respect to this real image the hologram behaves as a positive thin lens combined with a prism.

Thus by illuminating the hologram with a coherent plane wave, one not only reconstructs the scattered wavefront but also obtains a focused image of the object, which in this case is a

point source. In this respect the action of a hologram is similar to the action of a zone plate except that in the former case no secondary images are formed. The analogy between the action of a hologram and a zone plate was investigated by Rogers.[24]

4. An Alternative Reconstruction Procedure

In the previous section the reconstruction of the point aperature was made by illuminating the hologram with a plane wavefront parallel to it. An instructive alternative is to make the direction of the plane wave the same as that used during the exposure of the photographic plate to prepare the hologram. This is simply done by exposing the photographic plate, developing it,and then replacing it in the original position. The light scattered from the object is not allowed to illuminate the hologram. The situation is illustrated in Fig. 22.

The wavefront that reaches the hologram is now represented by $A_o \exp(-iax)$. As this wave passes through the hologram it is multiplied by the transmittance $\alpha(x)$ as given by equation (19). Again we distinguish three components of the radiation that emerge from the hologram. These are again separated at a sufficiently removed distance as can be seen from Fig. 22.

The first component is due to the first two (constant) terms of (19). Since this component is proportional to $\exp(-ax)i$ it will be identical to the incident wave except that it will have a smaller amplitude.

Fig. 22.-- Wavefront Reconstruction with obliquely incident plane wave. O' is the virtual image, O" is the real image.

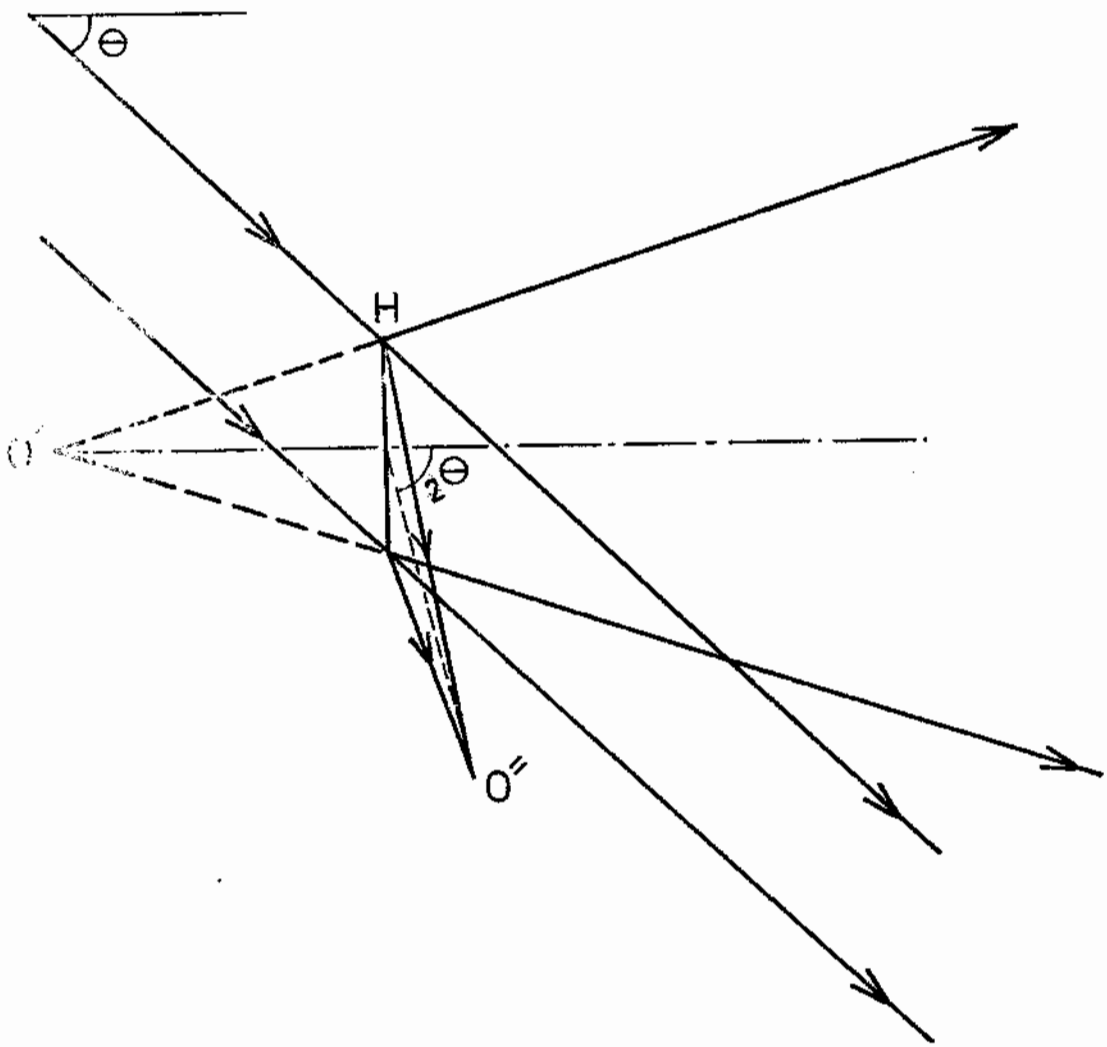

Fig. 22

The second component is produced by the third term of (19). When this term multiplies the incident wave the result is proportional to exp $(i \frac{\pi}{\lambda f} x^2)$. This represents a spherical wave identical in phase to the wave scattered from the object during the exposure of the hologram. It thus gives rise to a virtual image O' in exactly the original position of the object.

The third component which arises due to the last term of (19) is proportional to exp $-i(2ax + \frac{\pi}{\lambda f} x^2)$. This is the product of two factors. The factor exp $(-i \frac{\pi}{\lambda f} x^2)$ represents a convergent spherical wave which produces a real image O" of the point aperture at a distance f from the hologram. The factor linear in x causes this image to be formed in a direction making 2θ with the normal to the hologram (for small θ). This is illustrated in Fig. 22.

5. Wavefront Reconstruction by Diffuse Illumination

Leith and Upatnieks[29] have suggested placing a diffusing plate between the source (laser light) and the object during the preparation of the hologram. The object will then be illuminated with diffuse light. The hologram thus made has many interesting properties.

An objection which might be made is that the diffuser destroys the coherence of the light which makes a reconstruction impossible. However the property which is essential to wavefront reconstruction is not lost when coherent light emerges

from the diffuser. True, the light striking the object is no longer a simple wavefront but instead has complicated phase and amplitude variations from point to point. However, these phase and amplitude variations are invariant in time. This is the essential property that makes wavefront reconstruction possible.

If the hologram, prepared in the manner described above, is reconstructed with collimated coherent light two reconstructed images appear, one real and the other virtual. The remarkable thing is that the real and virtual reconstructed images are found to gain an interesting property. They can now be observed visually without an eyepiece or other visual aid. The virtual image can be seen by simply looking through the hologram as if it were a window. The real image may also be seen suspended in front of the hologram. Without the diffuser the reconstructions could not usually be observed in this fashion.

To explain the reason for this, consider a transparency which is illuminated with a point source. Except for some scattered light, the observer receives light from that part of the transparency which lies in the cone defined by the point source and the pupil of the eye. This is usually a small portion of the transparency. However, if a diffuser is placed behind the transparency, then light reaches the eye from all

parts of it and all the transparency can be seen without moving the eye.

Another interesting property of diffuse illumination follows from the fact that each point on the object illuminates the entire hologram. This means that the hologram plate may be broken into small parts and each part will reconstruct the whole object. However resolution is lost as the parts become small since the hologram is the limiting aperture of the wavefront reconstruction imaging process.

One of the most important properties of the hologram produced by diffuse illumination is that local imperfections in the optical elements no longer markedly degrade the reconstructed images. Before the introduction of the diffuse illumination technique, it has long been a familiar fact to experimentalists in holography (photography by reconstructed wavefronts) that any scratches or dust particles on the hologram recording plate, or on other elements of the optical system, produce troublesome diffraction patterns that appear in the reconstructed images. These could be minimized by careful technique but not completely eliminated. In the diffuse illumination holograms, such imperfections are practically absent from the reconstructed images. In fact diffuse illumination holograms could be scratched and handled roughly without noticeable degradation of images.

Some of the properties described above may be understood by recognizing the fact that the hologram represents a dispersion of the original object. By this we mean that each resolution element (detail) of the object is transformed into a function over the entire hologram plate. Such transformation is fundamental to all reconstruction techniques.[29] With diffuse illumination, the dispersion is much greater than is usual in previously used techniques. This explains why a small fragment of the diffuse illumination hologram contains information about the whole object.

So far, no rigorous analysis seems to have been given of the diffuse illumination reconstruction technique. Qualitatively we may say that the hologram of a diffusely illuminated object reconstructs not only the object but also the diffusing plate, which makes it possible for the observer to see the reconstructed image as if it were illuminated by a diffuse source.

IV. APPLICATIONS OF WAVEFRONT RECONSTRUCTION TO OPTICAL TESTING

A. Basic Concepts

An idea which should be useful in optical testing comes to mind on reconsidering the hologram reconstruction illustrated in Fig. 22. Assume, for the moment, that during the reconstruction, we allow the source to illuminate the point aperture also. In this case the hologram will be illuminated by two coherent waves: (a) the usual illuminating wave shown in Fig. 22; (b) the wave which emerges from the point aperture. As we have already seen, the plane wave, after being scattered by the hologram, yields a component which looks like the wave emerging from the point aperture. We have now to see what happens to the wave emerging from the aperture when it is scattered by the hologram. Reexamining the hologram transmittance equation (19), of Section III, we see this wave also will consist of three components. These, too, will be propagating in distinct directions and will, therefore, be separated at sufficient distance from the hologram. The component which concerns us now is the one which arises from the constant terms of equation (19). This will be identical to the reconstructed wavefront of center O' (Fig. 22) in all respects except, perhaps, amplitude. If an observer places his eye so as to receive light from these waves, he will see a uniformly illuminated field produced by interference of the two cophasal wavefronts.

Assuming that the same analysis holds for an extended object, as it must by the superposition principle, this idea may be applied to optical testing.

If an extended object in the form of, say, a lens is used in place of the point aperture and if a hologram is made of this object, one can at a later time observe interference fringes between wavefronts that come from the lens then, and those which emerged when the hologram was made. Alternatively, one can observe the interference fringes between the original lens and another by placing the latter, at the time of reconstruction, in the position which was occupied by the former at the time of producing the hologram. The above procedure allows the possibility of: (a) keeping track of the progress of a polishing operation by observing the changes in shape as polishing goes on: (b) comparing, interferometrically, an optical element with an accurate element which is no longer at hand; and (c) comparing the wavefront emerging from an optical element of one aperture with the one from a different aperture component.

B. Applications to Optical Testing

1. A Way of Testing a Spherical Mirror of Large Aperture

Consider the arrangement illustrated in Fig. 23. In this arrangement C is a point source formed by focusing the collimated light generated by a laser. This point source is at the center of curvature of a perfect spherical mirror M and also at the focus of the well-corrected lens L. Part of the spherical wave from C passes through the beam-splitter S and travels towards the mirror M

Fig. 23.--Testing a spherical mirror using the methods of wavefront reconstruction. C is the center of M and the focus of L.

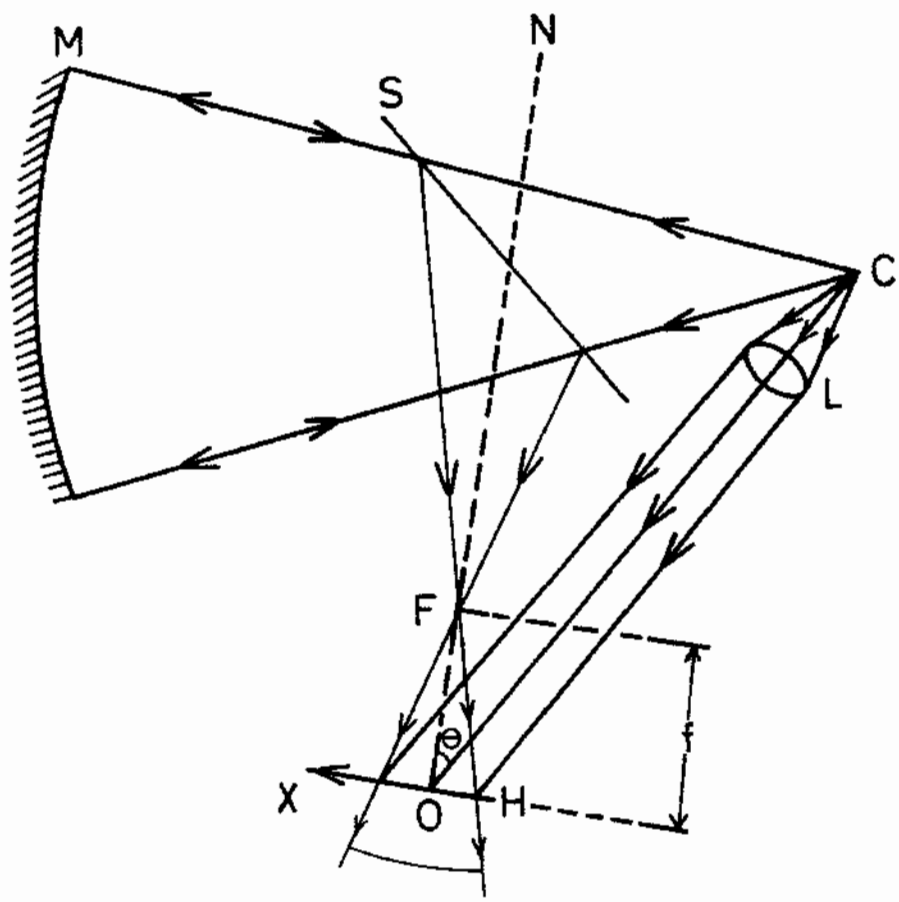

Fig. 23

where the wave is reflected back towards the beam-splitter which reflects part of the light. The wave reflected by S forms an image F and is received by the photographic plate H placed at a distance f from F.

Another part of the spherical wave from C is collimated by the well-corrected lens L and strikes the photographic plate obliquely, as shown in the figure, forming the reference beam.

The two coherent waves interfere at H. As the photographic plate is exposed and developed a hologram of the mirror M is formed. The transmittance $a(x)$ of the hologram will be given by Equation (19) of Section III, provided that the amplitude of the reference beam is much greater than the amplitude of the spherical wave that comes from F. It is easy to meet this requirement by controlling the silvering of S.

It is important to note the parameters which determine the phase of the reconstructed wavefront at any point x. These are 'a' which is a function of θ, and f. If these are given the phase of the reconstructed wavefront is determined.

From the discussion of Section IV-A we recall that if the photographic plate is developed and replaced then, with everything else as it is, an observer looking in the direction of F, from a distance sufficiently far, will see a uniformly illuminated field.

If M is replaced by an aspherical mirror then the observer will see an interference pattern which will depend on the departure of the mirror from sphericity.

If we do not have a perfect large aperture spherical mirror, as is usually the case, the problem of making the hologram in the plane is not insurmountable. The following method suggests itself.. The small aperture system illustrated in Fig. 24 can be used to produce the hologram of a perfect spherical mirror. In this arrangement S is a beam-splitter, L is a well-corrected lens and M is a good optically flat mirror. The hologram is formed at a distance f from the focus F of the lens L and with the reference beam making an angle θ with the normal to the hologram as shown in the figure.

Next we use the arrangement of Fig. 23 where now M is the spherical mirror to be tested. The center of curvature should be determined first (approximately) and the hologram, as prepared in the fashion of the previous paragraph, is placed at a distance f from the position of best focus F and with the proper orientation relative to the reference plane wave.

With the observer looking towards F from a sufficiently far position the interference pattern will reveal the quality of the mirror. For example, if a few fringes appear in the field then the mirror is only a few fringes from perfection. If a large number of fringes appear the quality of the mirror under test is still poor.

An advantage of this method is that the reference spherical wavefront that is implicitly used is produced by a small aperture system.

Fig. 24.--Preparation of a hologram to be used in the testing of a spherical mirror (schematic).

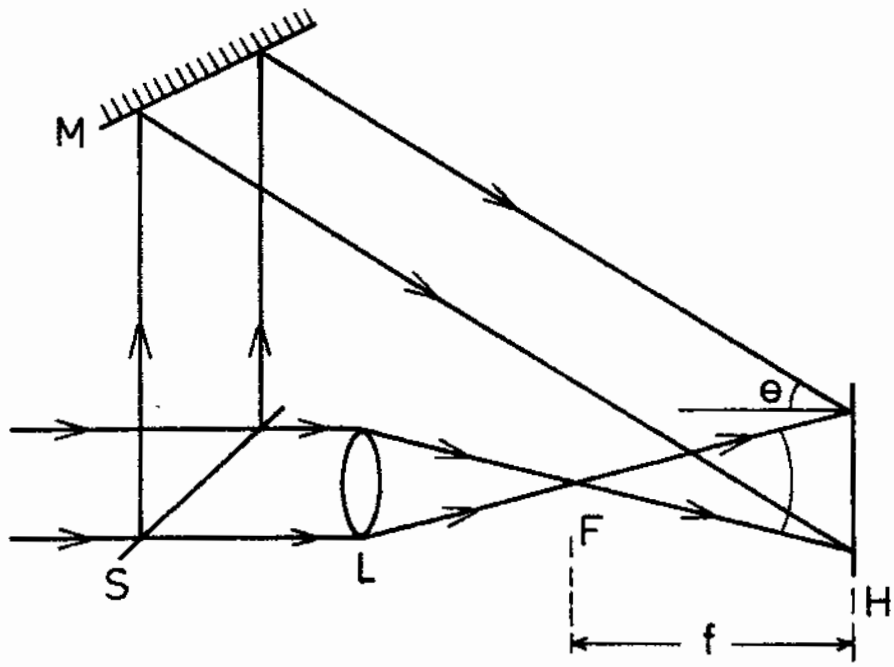

Fig. 24

2. Testing of an Aspheric Mirror Using an Artificially Produced Hologram

In this section we try to extend the idea of the previous section to the case of a general aspheric surface. The basic problem to be solved if one is to test an aspheric surface by wavefront reconstruction is the production of the hologram of the correct surface before the surface is produced. This is necessary so that the correct surface can be compared interferometrically with the actual surface which has been produced.

One way of solving this problem is the following. First, by ray tracing from a point source to the aspheric mirror desired and then to the plane of the hologram (see Fig. 23 where M is replaced by an aspheric mirror) one can determine the phase at the photographic plate of the wavefront reflected from M. It is then a simple matter to determine the location of the interference maxima of this wavefront with the reference wavefront. With this information, it is possible to make, on a large scale, a drawing of these interference maxima. This drawing can then be scaled photographically to the proper reduced size. The photograph prepared in this fashion is an artificially made hologram of the perfect aspheric surface.

To test an aspheric element of the previously determined design, the arrangement of Fig. 23 is used, where, now, M is the element to be examined and H is the hologram prepared in the

manner described above. As the observer looks through the hologram, from a proper position, interference fringes will show the difference between the actual element and the desired one.

It should be noted that the line drawing of the hologram will have the form of a high contrast negative hologram. The fact that gradual shading in the artificial hologram will be missing is of no consequence in determining the phase of the reconstructed wavefront, although it will have an effect on the intensity distribution. This can be seen from equation (17) of section III B-1, where it has already been noted that the magnitude of Γ is not important for the reconstruction.

In the interest of keeping the line spacing in the hologram as large as possible, it is desirable to choose θ (Fig. 23) quite small. The question of tolerance in the position of the lines of the drawn hologram remains to be investigated. However these tolerances should be no more severe than those of a zone plate.

REFERENCES

1. E.H. LINFOOT, Roy. Soc. of London Proc. A, 186, 72 (1946).
2. Ibid, 193, 248 (1948).
3. E.H. LINFOOT, Recent Advances in Optics (Oxford University Press, 1955), 128.
4. E. GAVIOLA, Opt. Soc. of Am. Journal, 29, 484 (1939).
5. C. CANDLER, Modern Interferometers (Hilger and Watts, 1951) 166.
6. S. TOLANSKY, Multiple-Beam Interferometers (Oxford University Press, 1948), 3.
7. J. STRONG, Concepts of Classical Optics (Freeman and Co., 1958), 229.
8. S. TOLANSKY, Roy. Soc. of London Proc. A, 184, 41 (1945).
9. A. MICHELSON, Studies in Optics (University of Chicago Press, 1928), 74.
10. Ref. 5, 139.
11. Ibid, 138.
12. Ibid, Chapters VI AND VII.
13. Ibid, 187.
14. W.J. BATES, Proc. of Phys. Soc. of London, 59, 940 (1947).
15. Nature, 158, 221 (1946).
16. M. BORN and E. WOLF, Principles of Optics (Pergamon, 1965), 316.
17. J.M. BURCH, Nature, 171, 889 (1953).
18. J. DYSON in Ref. 7, 383.
19. Ibid, 384.
20. J.B. SANDERS in Ref. 7, 393.

21. D. GABOR, Nature, 161, 777 (1948).

22. D. GABOR, Roy. Soc. of London Proc., A, 197, 454 (1949).

23. D. GABOR, Proc. of Phys. Soc. of London, B, 64, 449 (1951).

24. G.L. ROGERS and W.L. BRAGG, Nature 167, 190 (1951).

25. P. KIRKPATRICK and H. EL-SUM, Opt. Soc. of Am. Journal, 46, 825 (1956).

26. E. LEITH and J. UPATNIEKS, Physics Today, 18, No. 8, 29 (1965).

27. E. LEITH and J. UPATNIEKS, Opt. Soc. of Am. Journal, 52, 1123 (1962).

28. Ibid, 53, 137 (1963).

29. Ibid, 54, 1295 (1964).

30. G.W. STROKE and D.G. FALCONER, Phys. Lett. 13, 306 (1964).

31. Ibid, 15, 238 (1965).

32. G.W. STROKE, App. Phys. Lett. 6, 201 (1965).

33. G.W. STROKE, Introduction to Coherent Optics and Holography (Academic Press, 1966).